Hindawi
Advances in Condensed Matter Physics
Volume 2019, Article ID 2329168, 15 pages
https://doi.org/10.1155/2019/2329168

Review Article

Two-Dimensional Optical Metasurfaces: From Plasmons to Dielectrics

Bo Liu,[1] Kerui Song,[2] and Jiangnan Xiao [1]

[1]*Shanghai Key Lab of Modern Optical Systems, Terahertz Technology Innovation Research Institute, and Engineering Research Center of Optical Instrument and System, Ministry of Education, University of Shanghai for Science and Technology, Shanghai 200093, China*
[2]*School of Materials Science and Engineering, Central South University, Changsha,410012, China*

Correspondence should be addressed to Jiangnan Xiao; jiangnanxiao@usst.edu.cn

Received 19 June 2018; Revised 2 October 2018; Accepted 18 December 2018; Published 10 January 2019

Guest Editor: Qinghua Guo

Metasurfaces, kinds of planar ultrathin metamaterials, are able to modify the polarization, phase, and amplitude of physical fields of optical light by designed periodic subwavelength structures, attracting great interest in recent years. Based on the different type of the material, optical metasurfaces can be separated in two categories by the materials: one is metal and the other is dielectric. Metal metasurfaces rely on the surface plasma oscillations of subwavelength metal particles. Nevertheless, the loss caused by the metal structures has been a trouble, especially for devices working in transmit modes. The dielectric metasurfaces are based on the Faraday-Tyndall scattering of high-index dielectric light scattering particles. By reasonably designing the relevant parameters of the unit structure such as the size, direction, and shape, different functions of metasurfaces can realize and bring a wide range of applications. This article focuses on the metasurface concepts such as anomalous reflections and refractions and the working principle of different types of metasurfaces. Here, we briefly review the progress in developing optical over past few years and look into the near future.

1. Introduction

Optical elements are the basic unit of optical systems such as imaging, illumination, and communications [1, 2]. They can change the direction of light beam propagation and reshape the wavefront by modulating the amplitude, phase, and polarization of light. The conventional optical elements, such as lenses, wave plates, and light modulators, are transmitted primarily through the principles of refracting, reflection, absorption, or diffraction of light [3]. Wavefront shaping is realized by the gradual accumulation of phase in the propagation of components, which is closely related to the structure, refractive index, and dielectric constant of components. Due to the limited manipulation mechanism and material selection of conventional optical components, it is difficult to achieve high integration such as chip integration, ultrathin structure, wavelength control, and polarization control [4]. With the development of microfabrication technologies and computational electromagnetic fields, miniaturization of optical device and integration of optical system have gradually become the trend of future development. An artificially designed new type of optical material media has gradually attracted more and more attention of researchers. Further studies have found that the effective combination of medium and transform optics is expected to achieve its complete control of electromagnetic waves and has become a new method for the study of beam propagation control and interaction laws of light and matter.

The metamaterials consist of periodical subwavelength metals and medium structures, which are artificial microstructures with a specific order. Due to the influence of subwavelength structures and overall functional materials, supermaterials exhibit extraordinary electromagnetic properties [5]. Therefore, the ideal electromagnetic response and device function can be obtained by adjusting the basic unit structure of the material, thereby eliminating the material performance constraints of the conventional materials [6]. For the study of metamaterials, many scholars

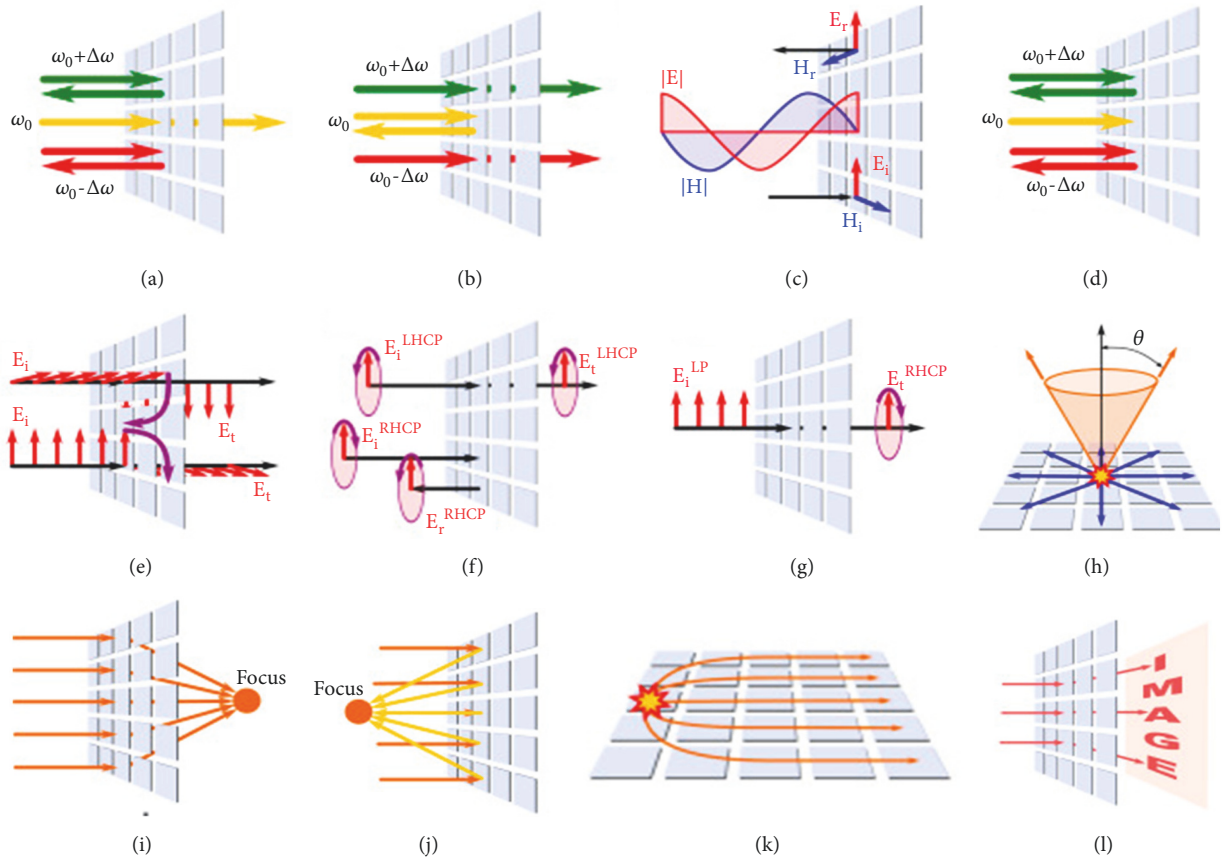

FIGURE 1: Selected functionalities of metasurfaces: (a) band pass frequency selective surface; (b) band stop frequency selective surface; (c) high-impedance surface; (d) narrowband perfect absorber; (e) twist polarizer; (f) right-handed circular-polarization frequency selective surface; (g) linear-to-circular polarization converter; (h) two-dimensional leaky-wave antenna with a conical-beam pattern; (i) focusing transmit array; (j) focusing reflect array; (k)flat Luneburg lens; (l) hologram [18].

have made major breakthroughs in different applications. So far, the metamaterials that have been obtained include negative-refractive-index materials [7–9], magnetic media [10], chiral materials [11–13], electromechanical metamaterials [14, 15], and photonic crystals [16], and they can be applied to some difficult areas of conventional optics, such as super-resolution imaging, electromagnetic cloaks, and all-optical devices [15]. With the deepening of research, resonance response and the use of metal structure leads to the existence of high loss and strong dispersion, which brings new challenges to practical application. In addition, micro-scale and nanoscale three-dimensional metamaterials are expensive and difficult to manufacture [17]. As a result, researchers have turned their attention to metasurfaces that are compatible with modern semiconductor. They can be easily fabricated using existing technologies such as photolithography and nanoprinting methods. At the same time, the ultra-thin thickness in the direction of wave propagation can significantly reduce undesirable losses by selecting suitable materials and metasurface structures [18]. In general, the metasurface can overcome the challenges of large-volume metamaterials and realize optical adjustment functions that are difficult with conventional optical devices. In conclusion, as shown in Figure 1 the study of metasurface has become one of the frontier in the field of metamaterials, which has important research significance.

The metasurface reduces the dependence on the propagation effect by introducing mutations in optical properties such as phase, amplitude, and polarization [3–5]. This mutation can be realized by a two-dimensional array of subwavelength scattering, which is an electromagnetic modulation primitive structure at the light wavelength called an optical antenna. Some common scattering structures include metal nanostructures, barbina structures, and high refractive index dielectric media nanomaterials. The core feature of the metasurface is the subwavelength distance between element structures, which can be different geometric parameters such as shape, size, and direction. Compared with the control of the light path of the metamaterial, the design of the metasurface is more focused on the wavefront control in the control of the light beam [26]. It realizes wavefront control by controlling the intensity and phase of each point, which avoids the loss of light through the cell structure multiple times, thereby strengthening the practical application. In addition, the metasurface has many advantages over conventional optical elements. First of all, the thickness of

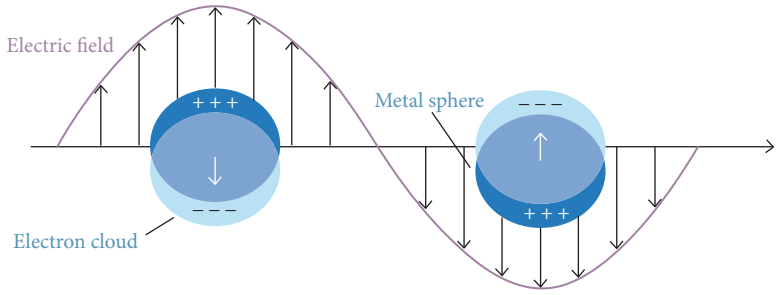

Figure 2: Schematic diagram of LSPs [19].

the metasurface is much smaller than the wavelength, so the treatment of transmitted light and reflected light occurs only in the structural layer where the interface is very thin. Secondly, due to the electromagnetic scattering characteristics, the metasurface can effectively control the optical phase, amplitude, and polarization at the subwavelength resolution and efficiently suppress high-order diffraction. Then the focus of the metasurface is not the far-field optical control, but the near-field wavefront shaping. Finally, the magnetic response of the metasurface can achieve impedance matching of planar optics, not just electric field responses like conventional elements.

In recent years, the field of metasurface research has developed rapidly and has achieved considerable research results. In this article, we review research progress abroad and summarize some research methods, thus presenting our own opinions on this research field.

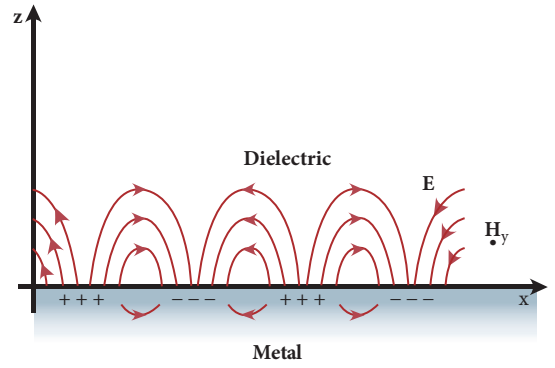

Figure 3: The electric field and the distribution of electric charges during the propagation of the SPPs in metal and dielectric interfaces [19].

2. Plasmonic Metasurface

2.1. Principle. The matasurface utilizes the phase jump introduced by the resonance of incident light with subwavelength structures. According to Huygen's Prindple, if it controls the amplitude and phase response of each "point source" (subwavelength structure) about the incident wave (electric field and magnetic field component) on the plane, the shape of the wavefront can be adjusted at will and achieve the devices expect performances. Similar to the case where the oscillator displacement is often out of sync with the excitation in the spring oscillator model, the phase jump is derived from the phase difference between the polarization charge displacement and the excitation field.

Plasmonic metasurfaces are generally consisted by metal nanoparticle structures and its substrate. When incident light reaches the metal nanoparticles, the free electrons on the surface will oscillate collectively, and called surface plasmons (SPs). There are two kinds of SPs, one of them produces charge density waves but they are unable to propagate, which became the localized surface plasmons (LSP), and the other transmits among the interface between the metal and dielectric, called surface plasmon polaritons (SPPs).

When light strikes the metal particles, free electrons on the surface exhibit directional movement, and form the electric dipole on the surface. Affected by electric dipole, free electrons on the surface of the metal particles produce resonance phenomenon, which strongly depends on their natural frequency of the harmonic vibration, the shape of geometry size, material properties, and dielectric environment surrounding metal particles [19]. Under the action of light with similar inherent frequency, metal particles formed the electronic collective oscillation, and the result is as shown in Figure 2.

Many nanostructures are capable of generating LSP resonances, such as common spherical and ellipsoidal metal nanoparticles, metal nanorods, and metal nanostars. Further, the coupling between the metal nanoparticles constituting the polymer can also cause LSP resonance, and a strong electric field is formed in the space between the respective units constituting the polymer. In addition, the metal nanopore structure can also generate LSP resonances, and the periodic metal nanopore structure can generate both LSP and SPPs along the metal surface. LSP can enhance local electric field, improve the efficiency of many optical processes, and have a wide range of applications in surface enhancement spectroscopy and biosensing.

SPPs are electromagnetic waves transmitted along the interface between metal and medium. They are exponentially attenuated in the direction perpendicular to the interface between the metal and the medium. Therefore, SPPs are locally distributed at the interface between the metal and the medium and spread in the subwavelength range, breaking through the diffraction limit. The principle of generating SPPs is shown in Figure 3.

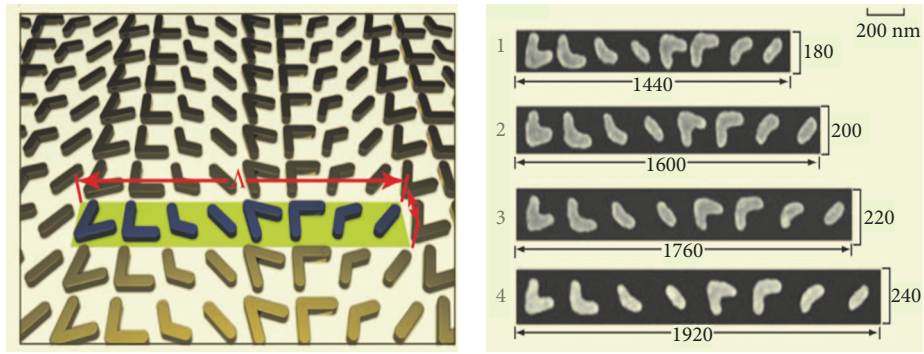

(a) (b)

Figure 4: Schematic representation of a nanoarray. (a) The unit (blue) at the plasmonic interface is composed of 8 metallic V-shaped antennas with a width of 40 nm and a thickness of 30 nm. The repetition period in the x direction is T, and the repetition period in the y direction is T/8. The phase delay of cross-polarized light increases from right to left along the x axis. (b) The scanning electron microscopy images of four antenna array cells with different cycles were produced on a single wafer.

In the field of midinfrared and optical wavelength research, researchers have proposed ultra-thin optical surface devices. Such new optical devices, called metasurfaces, control the polarization [5], phase, amplitude, and dispersion [17] of light by using the scattering properties of ultra-thin wavelength scale optical resonators at interfaces [27]. The designs use wavelength-scale dielectric or metallic nanoparticles to control dispersion characteristics in resonant scattering systems or in nonresonant situations, so as to make use of geometrical phase to control light scattering [28]. In recent years, the development of light field modulation has been increasing. For example, the generation and application of vortex and vector light have always been hot research [29–34]. Plasmons have also proven that they can be applicable to optical modulation [35], just like the generation of ring-shaped beams in carbon disulfide by using a graded-index plasmonic lens [36]. Metamaterials and plasmons have evolved a new revolutionary field in photonics by combining the energy and momentum of photons into a free electron gas in the form of a surface plasmon, which combines the properties of photonics and electronics [37]. Surface plasmons move on the metal surface and realize the transmission and operation of light at nanometer scale [9].

2.1.1. Nano-Array Antenna Metasurface. For a device with a discontinuity of phase at the interface and can be completely light-guided, its unparalleled control of abnormal reflections and refraction can be expressed in terms of the generalized Snell's law:

$$\sin(\theta_t)\, n_t - \sin(\theta_i)\, n_i = \frac{\lambda_0 \nabla \Phi}{2\pi} \quad (1)$$

$$\sin(\theta_r) - \sin(\theta_i) = \frac{n_i^{-1} \lambda_0 \nabla \Phi}{2\pi} \quad (2)$$

where θ_t, θ_i, and θ_r are the angle corresponding to refraction, incidence, and reflection, respectively; n_t and n_i stand for the refractive index of the two different media on the transmission and incident sides, respectively; λ_0 is the wavelength of free space. Equations (1) and (2) show that there is a gradient $\nabla\Phi$ at the discontinuity of the interface phase, the direction of light refraction and reflection can be changed by using components along the interface, and it can be implemented in an extremely thin layer. It is worth noting that, in essence, $\nabla\Phi$ is an added momentum contribution, which can be introduced by coupling the nanoantennas at the interface and destroying the symmetry at the interface; therefore, the light waves will be bent to achieve momentum conservation [38, 39]. The control of the degree of freedom of the light by the nanoantenna array is shown in Figure 4. Since the nanoantenna array is an ultra-thin structure, the metasurface function can be combined with the low-loss characteristics. This will hopefully achieve the production of a variety of optical components, making special light modulation and control possible.

If the interface was added to a periodic array of subwavelength resonators of negligible thickness forming a meatasurface, the reflection and transmission coefficients will be then dramatically changed because the boundary conditions are modified by the resonant excitation of an effective current within the metasurface. The reflection and transmission waves carry a phase change that can vary from $-\pi$ to π, depending on the wavelength of the incident wave relative to the metasurface resonance. When the resonators are anisotropic, the polarization state may be also altered. When the phase change is uniform along the interface, the directions of reflection and refraction are unaltered; in contrast, one of the merits provided by meatasurfaces is that we can create spatial phase variation with subwavelength resolution to effectively control the direction of wave propagation and the shape of wavefront [40].

The metasurface structure with symmetrical fracture V-shaped nanoantenna array achieves a mutated phase shift from zero to 2π on crossed polarized light, which can be devoted to design many planar optical elements [41]. Figure 5 shows the schematic diagram of some applications of optical metasurface. Just like in order to realize function of the lens, nanoantennas can be set to concentric rings. In a variety

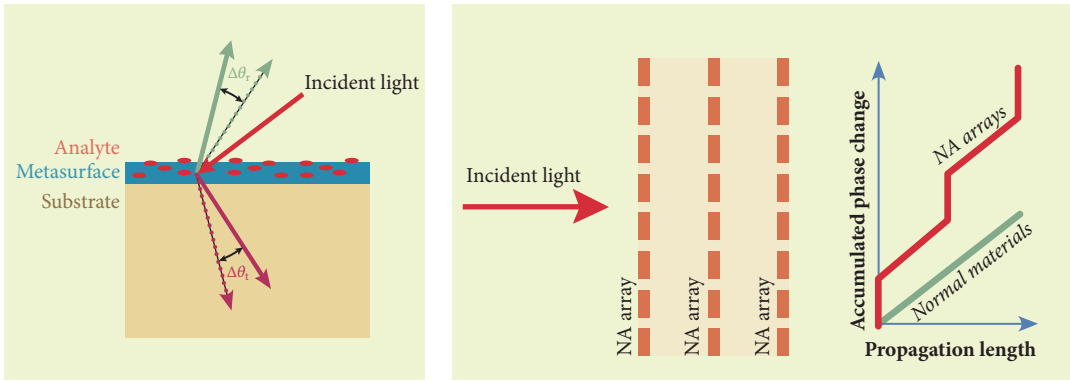

(a) (b)

Figure 5: Applications of optical metasurface. (a) Metasurface acts as a chemical sensor: the molecules are attached to the metasurface, resulting in the transfer of resonances of the nanoantennas components. This leads to anomalous reflection and transmission beam angle changes (indicated by $\Delta\theta_y$ and $\Delta\theta_t$, respectively). (b) Schematic diagram of a superrefractive index medium consisted of 3 metasurfaces (left panel). The right panel displays the cumulative phase transition of light passing through a common homogeneous material (green line) and through a medium consisting of 3 metasurfaces (red polyline), the slope of every red polyline representing the effective refractive index.

of different shapes, nanoantennas are arranged in such a way that the mutated phase shift leads to complete phase length interference on the distance f after wave propagation through the interface. This ultra-thin metal lens can be designed to generate a variety of beams, such as a nondiffraction bezier beam. Moreover, the plasmonic metasurface can control the phase of light, which makes it also applied to 3D optical holography [40].

2.2. Plasmonic Application

2.2.1. Optical Vortex Plates. According to the mutated phase of the interface [42, 43], a phase plate consisting of two-dimensional V-shaped metal plasmonic antennae [44, 45] is designed and produced to generate an optical vortex from cross-polarized scattered light of the modulator transmission. Then by controlling the geometry of the antenna and selecting the array element group, it covers the phase more than 2π radians. The first-order or second-order vortex phase plate is designed based on different topological charges, and different order vortex beams are finally generated [46, 47]. Figure 6 shows a vortex phase plate model with eight groups of plasmons and subwavelength antenna metasurface structures distributed in one azimuth.

In addition, the use of gradient metasurface can make vortex beam generator miniaturization [48, 49]. The continuous metasurface is composed of multicircular chirp plasmons surface waveguides with anisotropy and spatial heterogeneity that can generate spin-orbit interactions of photons. The surface plasmons waves of radial polarization are excited by continuous superstructure. When the chirp coefficient is zero, a vortex beam with a topological charge of 1 can be generated by irradiating a metasurface with a wavelength of 632.8 nm of left-handed polarized light and a vortex beam with a topological charge of 2 can be obtained by using the analyzer to detect the crossing polarization components in the radiation wave. When the chirp coefficient is not zero, the topological charges of the vortex beam change from an integer to a fraction. The use of a high refractive index material to further fill the annular chirp waveguide can theoretically generate vortex beams of arbitrary topological charges (integer and fractional). Moreover, compared with the discrete metasurface, the continuous metasurface "pixel points" can be infinitely small, high precision phase modulation can be achieved, and extremely pure vortex beam can be obtained.

2.2.2. Three-Dimensional Color Holography. A simple three-dimensional color hologram can be fabricated from a thin layer of metal with a thickness of only ten to a hundred nanometers [50]. Since its smallest pixel size is only 200nm × 200 nm, its projection holographic field of view can reach 90° (That is the entire transmission space is imaged) and even the evanescent wave area. Since the entire visible light band is an achromatic structure, full-color holographic imaging can be achieved by utilizing this structure and introducing off-axis illumination technology. The offaxis illumination technology introduced can eliminate the zero-order light interference and the cross-talk between different color images in traditional metasurface color holography, which greatly improves the imaging SNR. Further, by using its subwavelength-scale pixel size, a hologram without a false image can be obtained by rationally designing a moving related image existing in a conventional color holography technique to a disappearing wave region. Figure 7 shows the generation of a hologram using a metasurface holographic plate. This holographic technology provides a more efficient method for phase and amplitude design and reconstruction, providing a viable solution for a wide range of applications in the microscope, beam shaping, and entertainment industries [51–57].

2.2.3. Hyperbolic Lens. The hyperbolic lens is a flat lens with superconducting plane waves that can perfectly focused.

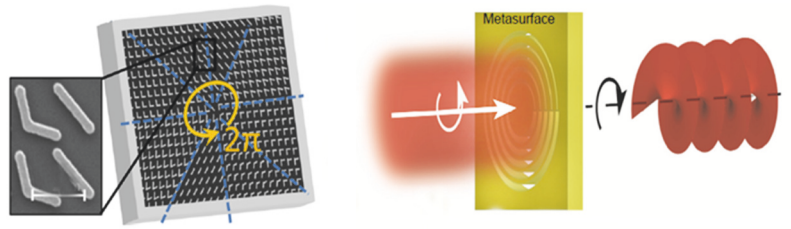

(a) (b)

FIGURE 6: (a) Eight groups of V-shaped focusing structures arranged in the radial direction of the circle, arranged along the azimuth direction with 0, $\pi/4$, $\pi/2$, $3\pi/4$, π, $5\pi/4$, 3π /2, and $7\pi/4$ phase antennas and linear spacing $\pi/4$. (b) Vortex phase mode.

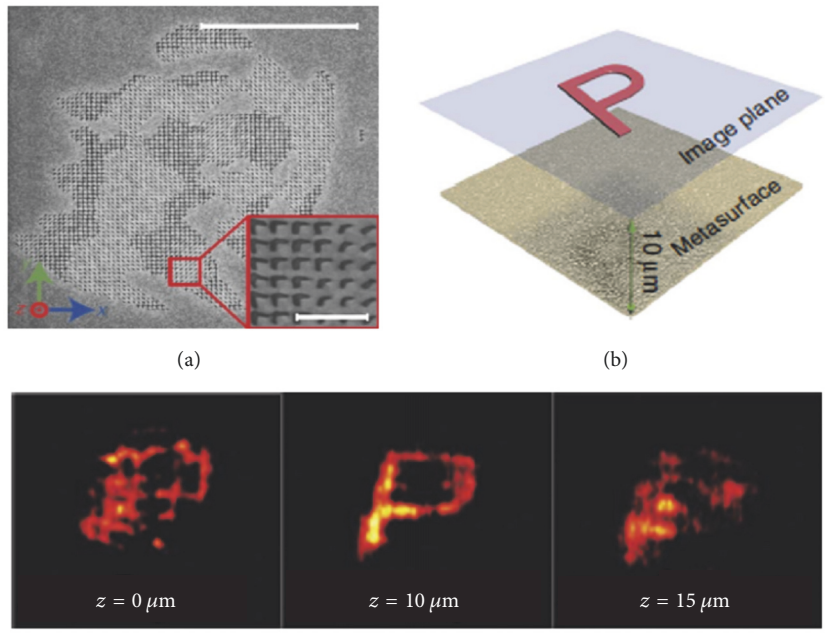

(a) (b)

(c)

FIGURE 7: (a) Place a pattern on a specific distance from the metasurface holographic plate (here we choose ten microns). (b) Create a specific holographic template on the metasurface. (c) Metasurface holograms received at a particular location.

Eight types of V-shaped focusing structures are periodically arranged in the radial direction of the planar circle. Each set of V-shaped focusing structures on the ring is evenly arranged. As shown in Figure 8(a), eight groups of V-shaped focusing structures are arranged in the radial direction of the circumference, and the phases are arranged from the inner ring to the outer ring to be 0, $\pi/4$, $\pi/2$, $3\pi/4$, π, $5\pi/4$, $3\pi/2$, and $7\pi/4$ antenna arrays and their phase linear spacing are $\pi/4$. Based on the perfect focus of the phase distribution, the arrangement of radial V-shaped structures was calculated, the position of each focusing structure r was determined, and finally the number of structures etched on the ring was obtained [58, 59]. By designing different microstructures, flat lenses with different focal lengths can be obtained. Due to the very thin thickness of the flat lenses, it is expected to be applied in the field of optical integration [60]. According to the above method, Figure 8(b) shows an ultra-thin flat lens that generates a specific focal spherical wave based on the metasurface structure.

3. Dielectric Metasurface

3.1. Principle. Unlike the plasmonic metasurface, the dielectric metasurface is formed by the distribution interface of high-refractive-index light scattering particles that is comparable to the wavelength of light [61–64]. The kind of scattering effect is called Faraday-Tyndall scattering. And when particles are cylindrical or spherical, the Helmholtz equation can be separated by boundary conditions, which matches the Mie scattering conditions [65]. Therefore, accurate Mie calculations are greatly helpful for dielectric nanoparticles. The radiation field and the internal field can be calculated by extending the solution to the spherical vector wave function. The analytical expression of the radiation field is generally

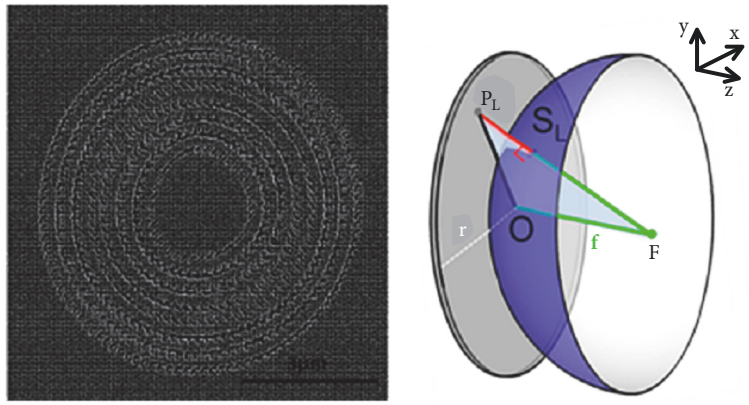

(a) (b)

Figure 8: (a) Lens model. (b) Schematic diagram of the ultra-thin flat lens producing a spherical wave of a specific focal length.

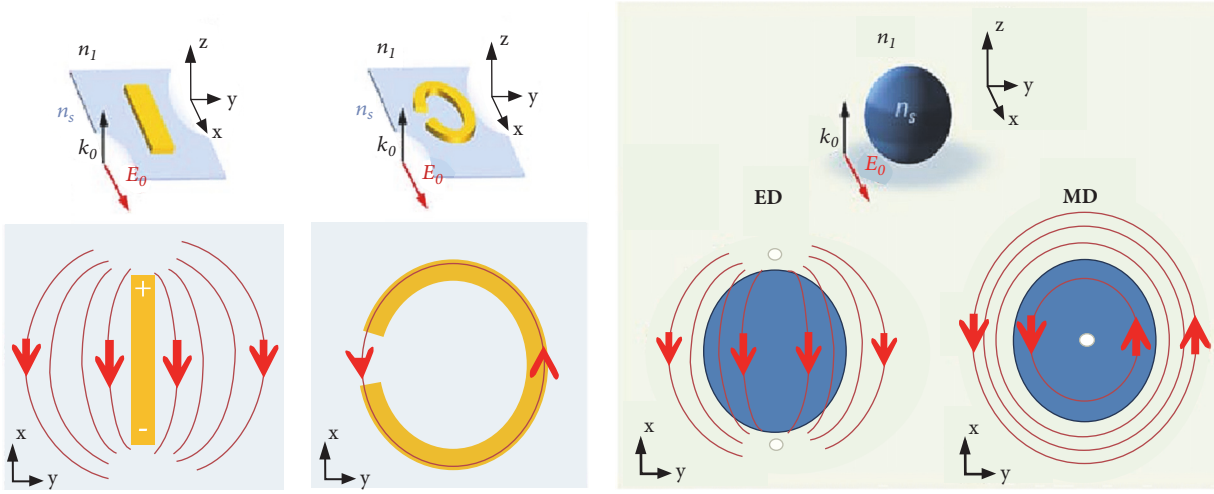

(a) (b) (c)

Figure 9: (a, b) Diagram of electric field in plasmonic resonator; (c) diagram of electric field in dielectric sphere. The plasmonic rod antennas only stand by electrical resonances and can ignore magnetic contributions. In plasmonic particles, metal rods are formed into a split ring resonator, which can realize strong magnetic dipole resonance [20].

compared with the experimental data, which can be fitted to extract the contribution of every model. And the analytical expression of the internal field stands for distribution of the field in the medium. It reveals the physical mechanism of efficient metasurface transmission or reflectivity.

If the spherical dielectric nanoparticles are small enough, they will undergo significant resonance in the electromagnetic field. In Figure 9, these resonances are mainly related to the excitation of magnetic and electric dipole modes. In description of Mie, the first resonance is magnetic dipole resonance in cases where the effective wavelength is the magnitude of the particle size ($\lambda_0/n_{sp} \approx D_{sp}$). Dipole magnetic resonance in a high refractive index dielectric resonator is virtually caused by an electric field rather than a magnetic field. As is shown in Figure 9(c), unlike metallic plasmonic nanoparticles, dielectric resonance is driven by displacement currents rather than electrical conduction currents, which greatly reduces the energy loss in resonance. It should be noted, as shown in Figures 9(a) and 9(b), that the polarization of the electric field in the metal cleaved ring resonator is antiparallel in both ends of the ring and can be effectively coupled to the cyclic displacement current.

Magnetic dipole modes also appear on aspherical geometry of dielectric particles. For example, in a single-layer cylindrical silicon resonator on a silicon-insulating substrate, the forced separation of the electrical and magnetic dipole resonances, as shown in Figure 10, enables the peak reflectivity in the short-wavelength infrared region to surpass 99%. In rectangular resonators, altering the size of the geometry or scattering makes tuning the resonant wavelength very easy [20]. The combination of electrical and magnetic resonance scattering properties is of great importance for achieving efficient planar optical metasurfaces.

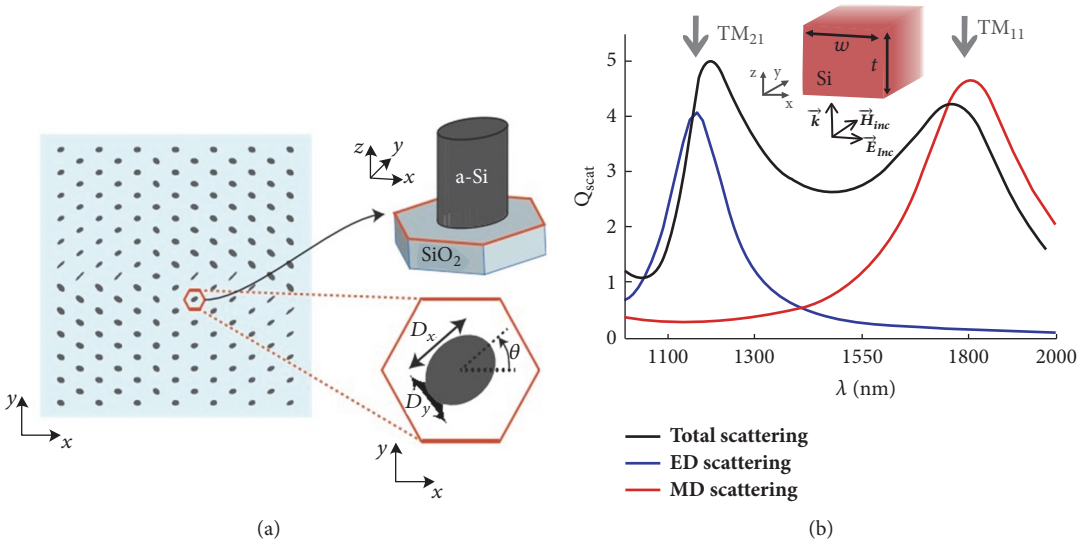

FIGURE 10: (a) The metasurface consists of an elliptic amorphous silicon column with the same height, different diameters (Dx and Dy), and different azimuthal angles (θ). The columns are located in the center of the hexagonal cell (pixel). (b) Rectangular dielectric nanoparticles also exhibit electromagnetic field polarizability. The figure shows the electric dipole (ED) and the magnetic dipole (MD) [20].

In order to further elucidate the potential of metasurface, considerable "electromagnetic field" scattering, we will introduce the study of Kerker *et al* here [66]. When the relative permittivity and relative permeability of the dielectric sphere are equal, *ie*, $\varepsilon = \mu$, zero backscatter and no depolarization are present. Because $\varepsilon = \mu$ particles scatter light and cause destructive interference in the backward direction. The effect described above is called the first Kerker condition [67]. When considering that the nanoparticles have a sufficiently small size until the size of particles are similar to the wavelength of the light, as a result, the prediction of Mie's scattered light coefficient will be greatly simplified, and the characteristics of the discrete field are left with only a few coefficients [68]. This means that nanoparticles can be considered as dipole particles; that is, only dipole conditions contribute to the scattering field.

For a better description of the electromagnetic field and magnetic dipole polarizability, two coefficients of the Mie extension can be introduced:

$$\alpha_e = \frac{3i\varepsilon}{2k^3} \quad \text{and} \quad \alpha_m = \frac{3i}{2\mu k^3} b_1 \tag{3}$$

where $k = n_{sp} k_0$.

Interference between the electric dipole and the magnetic dipole causes the appearance of a backscattering cross section, which can be expressed as

$$\sigma_s(\pi) = 4\pi k^4 \left(\left| \varepsilon^{-1} \alpha_e \right|^2 + \left| \mu \alpha_m \right|^2 \right) \left[1 + \cos(\pi - \Delta\phi_\alpha) \right] \tag{4}$$

When the dipole oscillates in phase ($\Delta\phi_\alpha = 0$), its minimum value is an overall mode comparable to the Huygens source.

The first Kerker condition has been widely used in the microwave and optical frequency bands of germanium, silicon, and gallium arsenide nanospheres.

Figure 11(a) shows a schematic diagram of the forward and backward radiation. Figure 11(b) also describes the scatter plots corresponding to the forward and backward radiation. In the pink/orange highlighted area of Figure 11(c), forward/backward scattering is acquired when the electrical and magnetic dipoles overlap at the common/antiphase resonance. This is achieved by a silicon nanodisk array embedded in a refractive index-optimized homogeneous medium in the Figure 11(d). In recent years, the wavelength-order nanopillar array in Figure 11(f) and the dielectric ridge waveguide made of amorphous silicon have been put forward as phase shift elements. Among these elements, an efficient transmission metasurface can be created at the midinfrared and infrared wavelengths as the wavelength distance propagates to the desired phase accumulation.

3.2. Dielectric Metasurface Applications. The dielectric metasurface is a new type of two-dimensional metamaterial, which has received more and more attention due to its ability to operate in light [62]. Compared with the phase transition induced by propagation in a conventional system, the metasurface can introduce phase and amplitude mutations through the optical resonator array [63]. In this respect, the dependence of the propagation effect can be simply released. Therefore, in the past few years, the characteristics of some novel two-dimensional devices have been gradually proposed and experimentally proved, such as abnormal

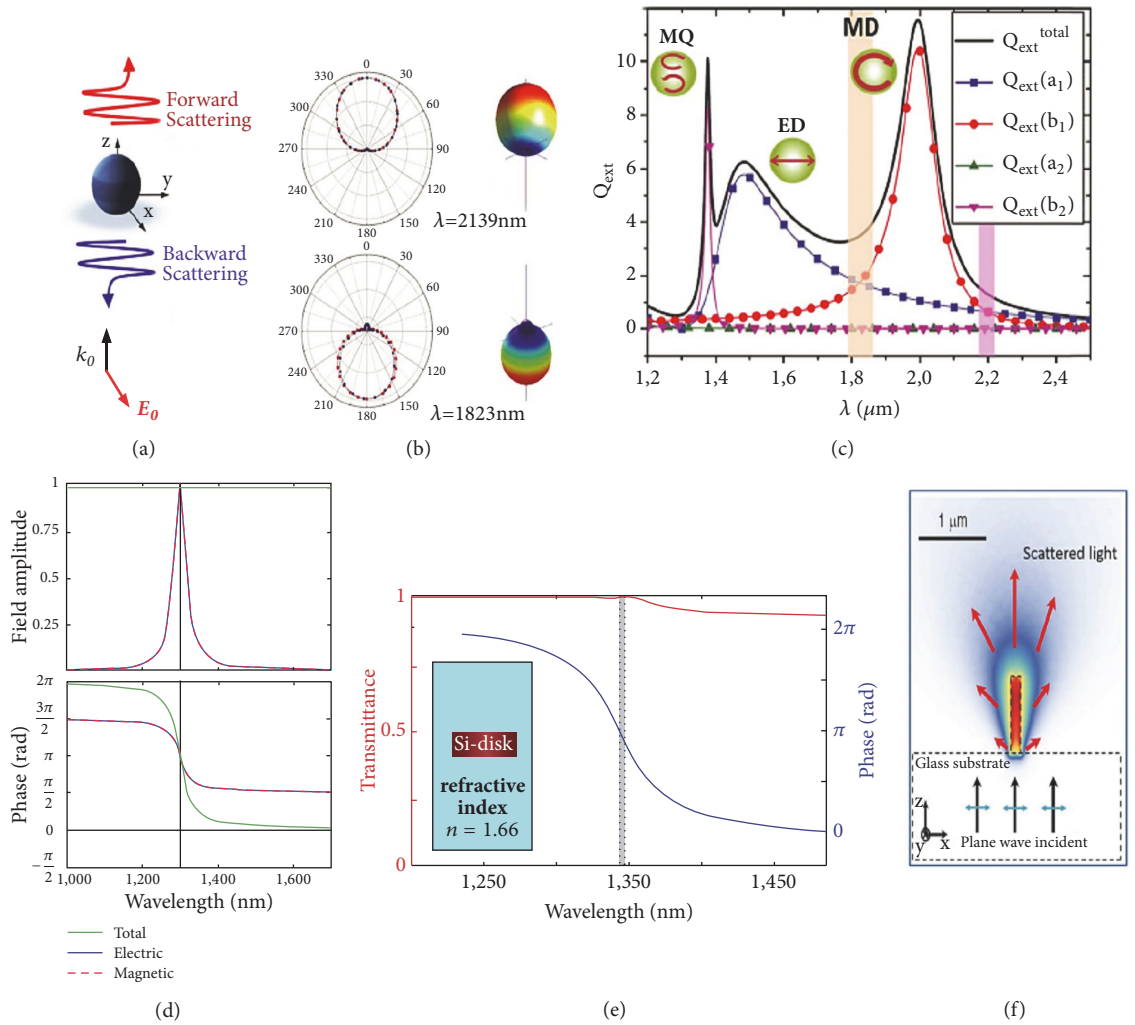

FIGURE 11: (a) Diagram of the forward and backscattering characteristic of micron-sized dielectric particles. (b) Scattering plot of a 240 nm germanium sphere; refractive index $n_{sp} = 4$ is a constant and positive value in this wavelength range. Two polarizations, parallel to the incident electric field (TM or p-polarization) or consistent with the plane of incidence (TE or s-polarization) are all considered. (c) The interaction of the total extinction profile Q_{ext} (black curve) with the wavelength is determined by the contribution of every parameter in the expansion of Mie [21]. The blue line corresponds to the contribution of the dipole and the red line to the contribution of the magnetic dipole, and approximately 1.4 microns pink depends on the magnetic quadrupole moment. (d) The phase and amplitude of the scattering field can be used as a function of wavelength of the ideal wavelength array, with electric and magnetic dipole resonance of the same intensity and width under plane wave illumination. (e) Numerical calculation of the transmission intensity (red line) and phase (blue line) of a silicon nanorod with a diameter of 484 nanometers and a height of 220 nanometers embedded in a homogeneous medium with the best optimal refractive index (n = 1.66). The resonance happens at a designed wavelength of approximately 1340 nanometers with a phase coverage of 2π. (f) Finite element simulation of the near-field distribution of scattered light in a circular amorphous silicon nanopillar (radius = 75 nm, height = 750 nm) as an example. (a, f) Corresponds to [22]; (b, c) Corresponds to [23]; (d, e) Corresponds to [24] adaptation.

reflection/refraction [64], surface-wave coupling [22], and high-resolution optical holograms [23]. Moreover, some of the plasmonic metasurfaces functions achieved can also be done by dielectric metasurfaces, like vector vortex beams generation [69], Pancharatnam-Berry phase lens and dynamical phase lens [70], etc.

3.2.1. High Impedance Metasurface. As shown in Figure 12, high impedance metasurface is a sandwich structure composed of subwavelength metal structure/dielectric layer/metal bottom plate, and it can almost completely reflect electromagnetic waves [71]. The structural elements of high impedance metasurface are much smaller than the working wavelength. According to the theory of equivalent circuit model, high impedance metasurface has equivalent inductance L and capacitance C, so the system has a specific resonant frequency. The equivalent impedance of a highly impedance metasurface is very high near the resonant frequency, which means that the horizontal magnetic field on its surface is very weak and the horizontal electric field is very strong, just like a "magnetic conductor." When the electromagnetic wave frequency is far away from the

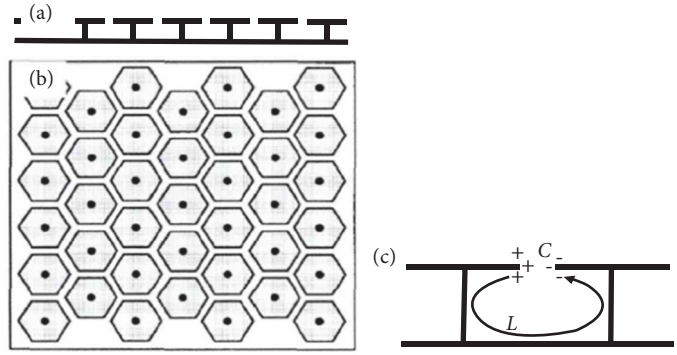

Figure 12: High impedance metasurface structure.

resonant frequency of the high impedance metasurface, the electromagnetic response of the system returns to the "magnetic conductor". These characteristics allow high impedance metasurface to have different reflective phases at different frequencies. At the resonance frequency of the system, the reflection phase is 0°, which means that even if the antenna is infinitely close to the high-impedance super surface, the antenna can maintain the same phase interference and the antenna has extremely high radiation efficiency. This characteristic of high impedance metasurface overcomes the disadvantage of one-fourth wavelength spacing limitation of traditional antenna baseplate, so that the antenna system can be miniaturized. When we classify this type of ultra-thin artificial micro-organisms in response to the special adjustment characteristics of electromagnetic waves on the electromagnetic surface, high-impedance metasurfaces are an important category.

3.2.2. Dielectric Gradient Metasurface. Gradient metasurfaces are two-dimensional optical elements capable of manipulating light by imparting local, space-variant phase changes on an incident electromagnetic wave. These surfaces have thus far been constructed from nanometallic optical antennas, and high diffraction efficiencies have been limited to operation in reflection mode. Erez Hasman's group have proposed a series of dielectric gradient metasurface optical elements capable of also achieving high efficiencies in transmission mode in the visible spectrum [25]. Ultrathin gratings [72–75], lenses [76, 77], and axicons have been realized by patterning a 100-nanometer-thick Si layer into a dense arrangement of Si nanobeam antennas. The use of semiconductors can broaden the general applicability of gradient metasurfaces, as they offer facile integration with electronics and can be realized by mature semiconductor fabrication technologies. Figure 13 shows an example of dielectric gradient metasurfaces optical elements (DGMOE).

3.2.3. Polarization-Controlled Metasurface. In 2007, Zhou Lei's research team proposed the perfect conversion of electromagnetic polarization using an anisotropic metasurface, which has no energy loss at all and can achieve 100% conversion efficiency [78]. As is shown in Figure 14(a), it is a sandwich structure composed of an "I" type metal structure/dielectric layer/metal with an ultra-thin structure [79].

Its equivalent dielectric model consists of an air layer, an anisotropic dielectric layer, and a metal layer. This anisotropic hypersurface has different resonant frequencies in the x and y directions. The system $\mu_{2xx} \longrightarrow \infty$ and $\mu_{2yy} \longrightarrow \infty$ at the x-resonance frequency means that, for x-polarized electromagnetic waves, the super surface appears as a "magnetic conductor" with a reflectivity of 1 and a reflection phase of 0°. For a y-polarized electromagnetic wave, the system response is an "electrical conductor" with a reflectivity of 1 and a 180° reflection phase. This expresses that after the incident electromagnetic wave is reflected by the metasurface, the x component of the electric field remains unchanged, and the y component of the electric field is reversed. Therefore, the polarization of the reflected wave is completely controlled in the vertical direction, achieving effective polarization conversion. On the other hand, this metasurface is comparable to an ultra-thin artificial birefringent material, so polarization control can be achieved. Compared with the conventional methods of polarization control, this kind of metasurface has the advantages of high efficiency and thin thickness. In addition, as shown in Figure 13(b), we also achieved effective polarization rotation in the optical frequency band [80], resulting in a perfect transmission 1/4 wave plate to achieve perfect polarization control of line offset, ellipsometry, and circular polarization [81].

3.2.4. Metasurface Prisms. The emergence of artificial electromagnetic specific media has triggered a series of revolutionary advances in light field control. According to a gradient-specific media system, metasurface devices operating in the microwave, terahertz, and optical bands have been designed. The gradient of the optical parameters of various special prisms and special prisms replaces the geometric gradients of conventional optics, and all of these optical controls fall into the category of volume control. With the V-shaped antenna array, people have designed a monochromatic phase-shift-free ultra-thin flat lens and prism axis [82] working in the communication band, which has opened up a new direction for the design of high numerical aperture, super-resolution planar prisms. Recently, we designed and

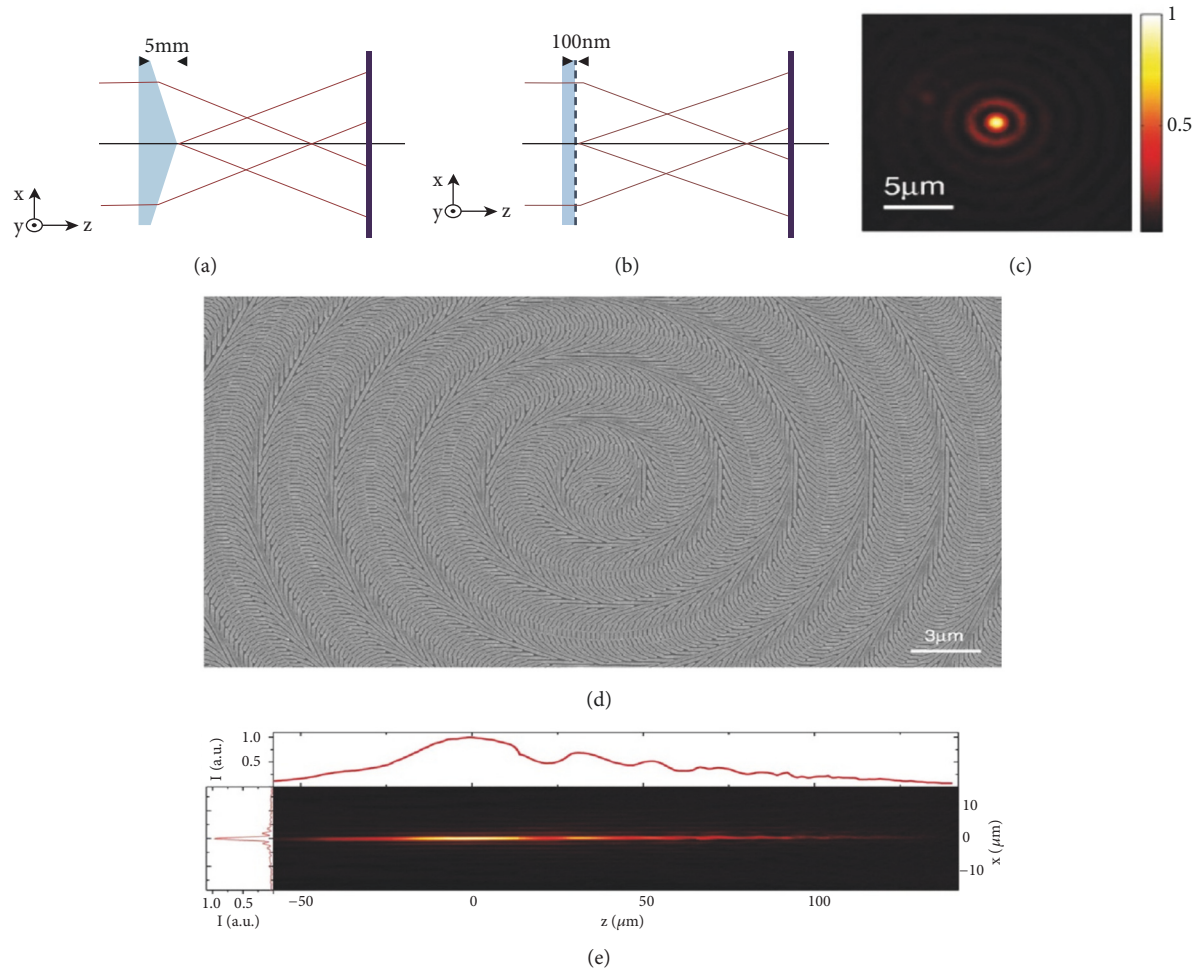

FIGURE 13: Example of a DGMOE: An axicon constructed from Si nanoantennas. (a) Schematic of a conventional glass axicon focusing light into a Bessel beam. (b) Schematic of a DGMOE axicon featuring an ultrathin patterned layer of silicon on a quartz substrate. (c) Transversal distribution of Bessel beam generated by the DGMOE. (d) SEM image of the fabricated DGMOE. (e) Measured intensity profile of the non-diffractive Bessel beam generated behind the DGMOE in the x and z plane. The intensity (I) along the center of Bessel beam is plotted in the inset along the z axis. The inset along the x axis shows the cross-sectional intensity profile at the z = 0 plane. a.u., arbitrary units [25].

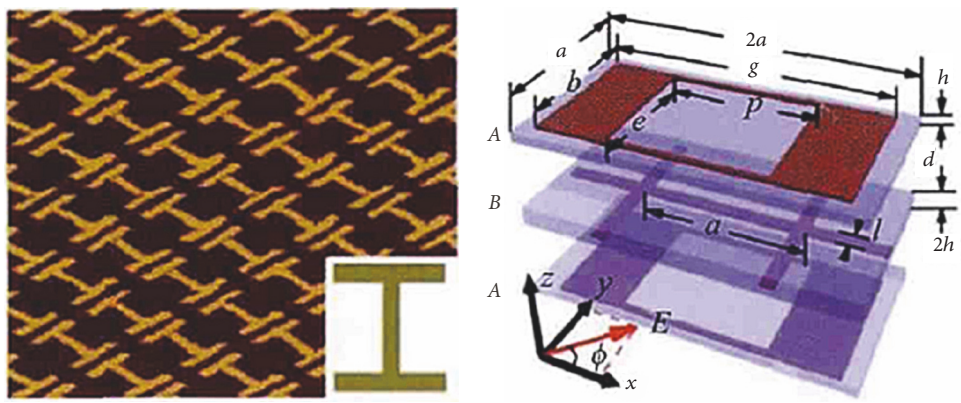

FIGURE 14: Polarization was controlled by reflection and transmission of metasurface structure. (a) Image of part of the experimental sample. (b) Geometry of the model systems.

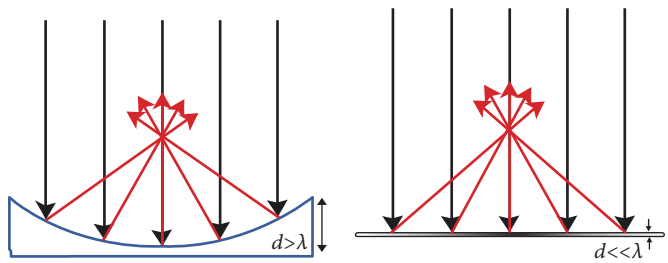

FIGURE 15: Metasurface prism's convergence effect. (a) Conventional optical device. (b) Metasurface prisms.

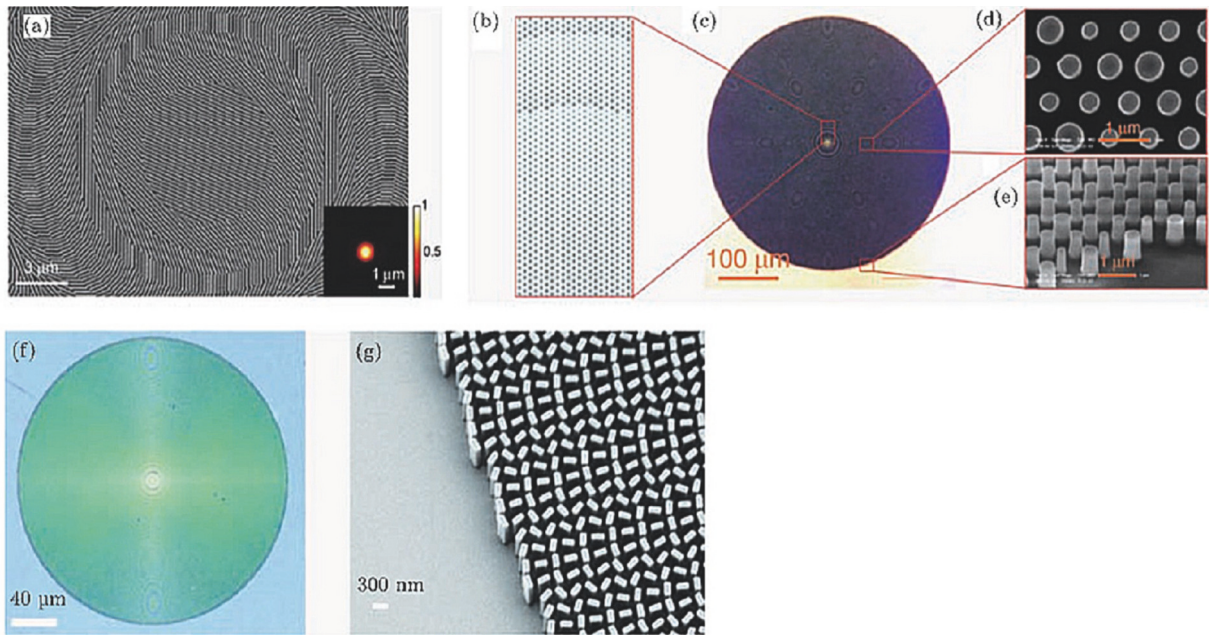

FIGURE 16: (a) All-media gradient metasurface lens. (b)-(e) High numerical aperture lenses; (f)-(g) visible light lenses.

fabricated a reflective gradient surface prism [83]. The incident plane wave's reflection phase distribution is hyperbolic. Experiments of Figure 15 show that the prism can focus incident light. The gradient metasurface prism thickness is much smaller than the wavelength (approximately $\lambda/20$) and all electromagnetic waves can be reflected and focused at the focal point. Therefore, with nearly 100% operating efficiency, it has important application value in the flat antenna.

3.2.5. Full Media Metasurface Lens. Metasurfaces based on all-dielectric nanostructures can overcome the limitations of plasmonic metasurface efficiency [20, 63–65]. Typically, the dielectric super surface is composed of a column of high refractive index media having a near wavelength length. The main types of materials include Si, TiO2, GaP, and SiN. In 2014, Brongersma et al. [1] of Stanford University proposed the concept of an all-dielectric metasurface, which provides an effective solution for designing efficient imaging lenses. The designed device is mainly based on the PB phase principle and uses silicon nanowires of sufficient depth. The structure is shown in Figure 16(a). When the incident light wavelength is about 500 nm, the focusing efficiency of the lens reaches 70%. In 2015, Faraon et al. [22] of California Institute of Technology designed a high numerical aperture lens with a round silicon column. The lens achieves 82% focusing efficiency at the 1550 nm communication wavelength. The microstructure is shown in Figures 16(b)–16(e). The circular silicon column has a high degree of rotational symmetry, so the designed lens is polarization-independent. The height of the silicon pillar is close to 1μm, the aspect ratio is relatively large, and the processing difficulty is also great. Although the proposal of dielectric metasurface is expected to solve the problem of plasmonic metasurface loss, the efficiency of the imaging lens designed in the visible light band is still limited, especially when the wavelength is 500 nm. In 2016, Capasso et al. [46] used PB phase to implement high-performance metasurface lenses in the visible region. As shown in Figures 16(f) and 16(g), the designed lens consists of a chloro-oxy dielectric rod and a glass substrate. A low loss medium material with smooth surface and high refractive index is used to solve the problem of material selection in visible band. Since this lens is based on the principle of PB phase

modulation, its main drawback is that circular polarized light must be used, so some additional devices are needed to deal with the light source.

4. Conclusion

In this paper, the typical plasmonic metasurface and the dielectric metasurface are introduced from two aspects: principle and application. The plasmonic metasurface consists of a periodic, subwavelength metal structure. We describe in detail the nanoantenna array structure that constitutes the plasmonic metasurface. By adjusting the different arrangements of the V-shaped antennas in the nanoantenna array, according to different abrupt phase shift methods, we introduced the application of the plasmonic metasurface in optical scroll plates, three-dimensional color holography, and hyperlenses. Then the advantages of dielectric metasurface are introduced: special control of electromagnetic wave and superiority of semiconductor materials. Based on this feature, the researchers achieved polarization conversion control with 100% conversion efficiency. Reflected gradient metasurface prisms can be used to reflect all electromagnetic waves and converge them at the focal point to achieve holographic imaging using a metasurface. Finally, we introduced a high numerical aperture all-media metasurface lens designed by researchers using low-loss dielectric materials. In a word, the plasmonic metasurface and the dielectric metasurface have their own advantages, and their applications are also very extensive. As a novel two-dimensional material, the metasurface has many secrets to be explored.

Conflicts of Interest

The authors declare that they have no conflicts of interest.

Acknowledgments

This work was supported by the National Natural Science Foundation of China (No. 61675048).

References

[1] N. Yu and F. Capasso, "Flat optics with designer metasurfaces," *Nature Materials*, vol. 13, no. 2, pp. 139–150, 2014.

[2] J. Wang and J. Du, "Plasmonic and dielectric metasurfaces: Design, Fabrication and Applications," *Applied Sciences (Switzerland)*, vol. 6, no. 9, p. 239, 2016.

[3] H.-T. Chen, A. J. Taylor, and N. Yu, "A review of metasurfaces: physics and applications," *Reports on Progress in Physics*, vol. 79, no. 7, Article ID 076401, 2016.

[4] N. Fang, H. Lee, C. Sun, and X. Zhang, "Sub-diffraction-limited optical imaging with a silver superlens," *Science*, vol. 308, no. 5721, pp. 534–537, 2005.

[5] T. Taubner, D. Korobkin, Y. Urzhumov, G. Shvets, and R. Hillenbrand, "Near-field microscopy through a SiC superlens," *Science*, vol. 313, no. 5793, p. 1595, 2006.

[6] J. Pendry, "Manipulating the near field with metamaterials," *Optics & Photonics News*, vol. 15, no. 9, pp. 32–37, 2004.

[7] D. R. Smith, J. B. Pendry, and M. C. K. Wiltshire, "Metamaterials and negative refractive index," *Science*, vol. 305, no. 5685, pp. 788–792, 2004.

[8] V. M. Shalaev, "Optical negative-index metamaterials," *Nature Photonics*, vol. 1, no. 1, pp. 41–48, 2007.

[9] R. A. Shelby, D. R. Smith, and S. Schultz, "Experimental verification of a negative index of refraction," *Science*, vol. 292, no. 5514, pp. 77–79, 2001.

[10] J. C. Wyant, C. L. Koliopoulos, and B. Bhushan, "An Optical Profilometer for Surface Characterization of Magnetic Media," *ASLE Transactions*, vol. 27, no. 2, pp. 101–113, 1984.

[11] J. Pendry, "Left-Handed Materials: Positively Negative," in *APS March Meeting*, 2004.

[12] E. Plum, V. A. Fedotov, and N. I. Zheludev, "Optical activity in extrinsically chiral metamaterial," *Applied Physics Letters*, vol. 93, no. 19, p. 1353, 2008.

[13] V. A. Fedotov, E. Plum, Y. Chen, A. S. Schwanecke, and N. I. Zheludev, "Chiral Photonic Metamaterial," in *Proceedings of the 2007 Quantum Electronics and Laser Science Conference*, pp. 1-2, Baltimore, MD, USA, May 2007.

[14] J. Y. Ou, E. Plum, L. D. Jiang, and N. I. Zheludev, "Nano-electromechanical switchable photonic metamaterials," *Metamaterials*, 2011.

[15] X. Fang, K. F. MacDonald, and N. I. Zheludev, "Controlling light with light using coherent metadevices: All-optical transistor, summator and invertor," *Light: Science & Applications*, vol. 4, no. 5, p. e292, 2015.

[16] S. Johnson, A. Mekis, S. Fan, and J. Joannopoulos, "Molding the flow of light," *Computing in Science & Engineering*, vol. 3, no. 6, pp. 38–47, 2008.

[17] Z. Liu, H. Lee, Y. Xiong, C. Sun, and X. Zhang, "Far-field optical hyperlens magnifying sub-diffraction-limited objects," *Science*, vol. 315, no. 5819, p. 1686, 2007.

[18] S. B. Glybovski, S. A. Tretyakov, P. A. Belov, Y. S. Kivshar, and C. R. Simovski, "Metasurfaces: from microwaves to visible," *Physics Reports*, vol. 634, pp. 1–72, 2016.

[19] K. L. Kelly, E. Coronado, L. L. Zhao, and G. C. Schatz, "The optical properties of metal nanoparticles: the influence of size, shape, and dielectric environment," *The Journal of Physical Chemistry B*, vol. 107, no. 3, pp. 668–677, 2003.

[20] F. Aieta, M. A. Kats, P. Genevet, and F. Capasso, "Multiwavelength achromatic metasurfaces by dispersive phase compensation," *Science*, vol. 347, no. 6228, pp. 1342–1345, 2015.

[21] P. A. Bobbert and J. Vlieger, "Light scattering by a sphere on a substrate," *Physica A: Statistical Mechanics and its Applications*, vol. 137, no. 1-2, pp. 209–242, 1986.

[22] A. Arbabi, Y. Horie, M. Bagheri, and A. Faraon, "Dielectric metasurfaces for complete control of phase and polarization with subwavelength spatial resolution and high transmission," *Nature Nanotechnology*, vol. 10, no. 11, pp. 937–943, 2015.

[23] R. Gómezmedina, B. Garcia Camara, I. Suarez-Lacalle et al., "Electric and magnetic dipolar response of Germanium spheres: Interference effects, scattering anisotropy and optical forces," *Physics*, vol. 5, no. 1, pp. 30–32, 2011.

[24] M. Decker, I. Staude, M. Falkner et al., "High-Efficiency Dielectric Huygens' Surfaces," *Advanced Optical Materials*, vol. 3, no. 6, pp. 813–820, 2015.

[25] D. Lin, P. Fan, E. Hasman, and M. L. Brongersma, "Dielectric gradient metasurface optical elements," *Science*, vol. 345, no. 6194, pp. 298–302, 2014.

[26] D. Veksler, E. Maguid, N. Shitrit, D. Ozeri, V. Kleiner, and E. Hasman, "Multiple wavefront shaping by metasurface based on mixed random antenna groups," *ACS Photonics*, vol. 2, no. 5, pp. 661–667, 2015.

[27] P. Genevet, F. Capasso, F. Aieta, M. Khorasaninejad, and R. Devlin, "Recent advances in planar optics: From plasmonic to dielectric metasurfaces," *Optica*, vol. 4, no. 1, pp. 139–152, 2017.

[28] W. Cai, D. A. Genov, and V. M. Shalaev, "Superlens based on metal-dielectric composites," *Physical Review B: Condensed Matter and Materials Physics*, vol. 72, no. 19, p. 193101(1-4), 2005.

[29] Y. He, Y. Li, J. Liu et al., "Switchable phase and polarization singular beams generation using dielectric metasurfaces," *Scientific Reports*, vol. 7, no. 1, 2017.

[30] M. Su, J. Liu, Y. He, S. Chen, and Y. Li, "Optical Orbital Angular Momentum Demultiplexing and Channel Equalization by Using Equalizing Dammann Vortex Grating," *Advances in Condensed Matter Physics*, vol. 2017, no. 2, pp. 1–9, 2017.

[31] Y. He, J. Liu, Z. Xie et al., "Independently detect the spiral phase of cylindrical vector vortex beams," in *Proceedings of the 2017 Opto-Electronics and Communications Conference (OECC) and Photonics Global Conference (PGC)*, pp. 1–4, Singapore, July 2017.

[32] X. Zhang, Y. He, Y. Cai et al., "Coherent Separation Detection for Orbital Angular Momentum Multiplexing in Free-Space Optical Communications," *IEEE Photonics Journal*, vol. 9, no. 3, pp. 1–11, 2017.

[33] X. Zhang, Y. Li, Y. Cai, M. Su, Y. He, and S. Chen, "Generating fast switchable optical vortices by beam combining," in *Proceedings of the 2017 Conference on Lasers and Electro-Optics Pacific Rim, CLEO-PR 2017*, pp. 1–4, Singapore, August 2017.

[34] Y. He, H. Ye, J. Liu et al., "Order-Controllable Cylindrical Vector Vortex Beam Generation by Using Spatial Light Modulator and Cascaded Metasurfaces," *IEEE Photonics Journal*, vol. 9, no. 5, pp. 1–10, 2017.

[35] C. Tan, X. Fu, Y. Hu et al., "Plasma optical modulation for lasers based on the plasma induced by femtosecond pulses," *Optics Express*, vol. 25, no. 13, pp. 14065–14076, 2017.

[36] C. Tan, Q. Wang, and X. Fu, "Topological insulator Sb2Te3 as an optical media for the generation of ring-shaped beams," *Optical Materials Express* , vol. 4, no. 10, pp. 2016–2025, 2014.

[37] Z. Jacob, L. V. Alekseyev, and E. Narimanov, "Optical hyperlens: far-field imaging beyond the diffraction limit," *Optics Express*, vol. 14, no. 18, pp. 8247–8256, 2006.

[38] D. Schurig, J. J. Mock, B. J. Justice et al., "Metamaterial electromagnetic cloak at microwave frequencies," *Science*, vol. 314, no. 5801, pp. 977–980, 2006.

[39] N. Yu, P. Genevet, M. A. Kats et al., "Light propagation with phase discontinuities: Generalized laws of reflection and refraction," *Science*, vol. 334, no. 6054, pp. 333–337, 2011.

[40] M. A. Kats, R. Blanchard, P. Genevet, and F. Capasso, "Nanometre optical coatings based on strong interference effects in highly absorbing media," *Nature Materials*, vol. 12, no. 1, pp. 20–24, 2013.

[41] C. L. Holloway, E. F. Kuester, J. A. Gordon, J. O'Hara, J. Booth, and D. R. Smith, "An overview of the theory and applications of metasurfaces: The two-dimensional equivalents of metamaterials," *IEEE Antennas and Propagation Magazine*, vol. 54, no. 2, pp. 10–35, 2012.

[42] A. V. Kildishev, A. Boltasseva, and V. M. Shalaev, "Planar photonics with metasurfaces," *Science*, vol. 339, no. 6125, p. 1289, 2013.

[43] N. Yu, P. Genevet, and F. Aieta, "Flat optics: controlling wavefronts with optical antenna metasurfaces," *IEEE Journal of Selected Topics in Quantum Electronics*, vol. 19, no. 3, Article ID 4700423, 2013.

[44] P. Bharadwaj, B. Deutsch, and L. Novotny, "Optical Antennas," *Advances in Optics and Photonics*, vol. 1, no. 3, pp. 438–483, 2009.

[45] L. Novotny and N. V. Hulst, "Antennas for light," *Nature Photonics*, vol. 5, no. 2, p. 83, 2011.

[46] E. H. Khoo, E. P. Li, and K. B. Crozier, "Plasmonic wave plate based on subwavelength nanoslits," *Optics Expresss*, vol. 36, no. 13, pp. 2498–2500, 2011.

[47] F. Aieta, P. Genevet, N. Yu, M. A. Kats, Z. Gaburro, and F. Capasso, "Out-of-plane reflection and refraction of light by anisotropic optical antenna metasurfaces with phase discontinuities," *Nano Letters*, vol. 12, no. 3, pp. 1702–1706, 2012.

[48] Y. Yang, W. Wang, P. Moitra, I. I. Kravchenko, D. P. Briggs, and J. Valentine, "Dielectric meta-reflectarray for broadband linear polarization conversion and optical vortex generation," *Nano Letters*, vol. 14, no. 3, pp. 1394–1399, 2014.

[49] H. Liu, M. Q. Mehmood, K. Huang et al., "Twisted focusing of optical vortices with broadband flat spiral zone plates," *Advanced Optical Materials*, vol. 2, no. 12, pp. 1193–1198, 2015.

[50] B. Desiatov, N. Mazurski, Y. Fainman, and U. Levy, "Polarization selective beam shaping using nanoscale dielectric metasurfaces," *Optics Express*, vol. 23, no. 17, pp. 22611–22618, 2015.

[51] R. Blanchard, G. Aoust, P. Genevet et al., "Modeling nanoscale V-shaped antennas for the design of optical phased arrays," *Physical Review B: Condensed Matter and Materials Physics*, vol. 85, no. 15, pp. 1745–1751, 2012.

[52] X. Yang, J. Yao, J. Rho, X. Yin, and X. Zhang, "Experimental realization of three-dimensional indefinite cavities at the nanoscale with anomalous scaling laws," *Nature Photonics*, vol. 6, no. 7, pp. 450–454, 2012.

[53] L. Huang, X. Chen, H. Mühlenbernd et al., "Three-dimensional optical holography using a plasmonic metasurface," *Nature Communications*, vol. 4, no. 7, article no. 3808, 2013.

[54] C. L. Holloway, A. Dienstfrey, E. F. Kuester, J. F. O'Hara, A. K. Azad, and A. J. Taylor, "A discussion on the interpretation and characterization of metafilms/metasurfaces: The two-dimensional equivalent of metamaterials," *Metamaterials*, vol. 3, no. 2, pp. 100–112, 2009.

[55] M. I. Shalaev, J. Sun, A. Tsukernik, A. Pandey, K. Nikolskiy, and N. M. Litchinitser, "High-Efficiency All-Dielectric Metasurfaces for Ultracompact Beam Manipulation in Transmission Mode," *Nano Letters*, vol. 15, no. 9, pp. 6261–6266, 2015.

[56] P. Genevet, N. Yu, F. Aieta et al., "Ultra-thin plasmonic optical vortex plate based on phase discontinuities," *Applied Physics Letters*, vol. 100, no. 1, Article ID 013101, p. 169, 2012.

[57] J. He, X. Wang, D. Hu et al., "Generation and evolution of the terahertz vortex beam," *Optics Express*, vol. 21, no. 17, pp. 20230–20239, 2013.

[58] F. Qin, L. Ding, L. Zhang et al., "Hybrid bilayer plasmonic metasurface efficiently manipulates visible light," *Science Advances*, vol. 2, no. 1, p. e1501168, 2016.

[59] W. Mo, X. Wei, K. Wang, Y. Li, and J. Liu, "Ultrathin flexible terahertz polarization converter based on metasurfaces," *Optics Express*, vol. 24, no. 12, pp. 13621–13627, 2016.

[60] Y. Guo, M. Pu, Z. Zhao et al., "Merging Geometric Phase and Plasmon Retardation Phase in Continuously Shaped Metasurfaces for Arbitrary Orbital Angular Momentum Generation," *ACS Photonics*, vol. 3, no. 11, pp. 2022–2029, 2016.

[61] F. Bouchard, I. De Leon, S. A. Schulz, J. Upham, E. Karimi, and R. W. Boyd, "Optical spin-to-orbital angular momentum conversion in ultra-thin metasurfaces with arbitrary topological charges," *Applied Physics Letters*, vol. 105, no. 10, pp. 36–262, 2014.

[62] X. Li, L. Chen, Y. Li et al., "Multicolor 3D meta-holography by broadband plasmonic modulation," *Science Advances*, vol. 2, no. 11, p. e1601102, 2016.

[63] A. W. Lohmann and D. P. Paris, "Binary fraunhofer holograms, generated by computer," *Applied Optics*, vol. 6, no. 10, pp. 1739–1748, 1967.

[64] B. R. Brown and A. W. Lohmann, "Computer-generated Binary Holograms," *Ibm Journal of Research Development*, vol. 13, no. 2, pp. 160–168, 1969.

[65] G. Mie, "Beiträge zur Optik trüber Medien, speziell kolloidaler Metallösungen," *Annalen der Physik*, vol. 330, no. 3, pp. 377–445, 1908.

[66] M. Kerker, *The Scattering of Light and Other Electromagnetic Radiation*, vol. 22, no. 5, pp. 620–645, 1969.

[67] M. Kerker, D.-S. Wang, and H. Chew, "Surface enhanced raman scattering (sers) by molecules adsorbed at spherical particles: Errata," *Applied Optics*, vol. 19, no. 24, pp. 4159–4174, 1980.

[68] B. Gompf and R. Pecha, "Mie scattering from a sonoluminescing bubble with high spatial and temporal resolution," *Physical Review E: Statistical Physics, Plasmas, Fluids, and Related Interdisciplinary Topics*, vol. 61, no. 5, pp. 5253–5256, 2000.

[69] X. Yi, X. Ling, Z. Zhang et al., "Generation of cylindrical vector vortex beams by two cascaded metasurfaces," *Optics Express*, vol. 22, no. 14, pp. 17207–17215, 2014.

[70] Y. Ke, Y. Liu, J. Zhou, Y. Liu, H. Luo, and S. Wen, "Optical integration of Pancharatnam-Berry phase lens and dynamical phase lens," *Applied Physics Letters*, vol. 108, no. 10, p. 45, 2016.

[71] Y.-W. Huang, W. T. Chen, W.-Y. Tsai et al., "Aluminum plasmonic multicolor meta-Hologram," *Nano Letters*, vol. 15, no. 5, pp. 3122–3127, 2015.

[72] Z. Bomzon, V. Kleiner, and E. Hasman, "Space-Variant Polarization-State Manipulation with Computer-Generated Subwavelength Gratings," *Micromachining and Microfabrication*, 2003.

[73] A. Niv, G. Biener, V. Kleiner, and E. Hasman, "Spiral phase elements obtained by use of discrete space-variant subwavelength gratings," *Optics Communications*, vol. 251, no. 4-6, pp. 306–314, 2005.

[74] G. Biener, A. Niv, V. Kleiner, and E. Hasman, "Space-Variant Polarization Scrambling for Image Encryption Obtained with Subwavelength Gratings," in *Proceedings of the 2005 Conference on Lasers and Electro-Optics (CLEO)*, Baltimore, MD, USA, May 2005.

[75] Z. Bomzon, G. Biener, V. Kleiner, and E. Hasman, "Vectorial Vortex Structures Formed by Computer-Generated Space-Variant Dielectric Subwavelength Gratings," Lasers & Electro-optics, Cleo 02 Technical Digest Summaries of Papers, 2002.

[76] A. L. Holsteen, D. Lin, E. Maguid et al., "Polarization-Independent Metasurface Lens Employing The Pancharatnam-Berry Phase," 2018.

[77] Y. Gorodetski, G. Biener, A. Niv, V. Kleiner, and E. Hasman, "Optical properties of polarization-dependent geometric phase elements with partially polarized light," *Optics Communications*, vol. 266, no. 2, pp. 365–375, 2006.

[78] J. Hao, Y. Yuan, L. Ran et al., "Manipulating electromagnetic wave polarizations by anisotropic metamaterials," *Physical Review Letters*, vol. 99, no. 6, Article ID 063908, 2007.

[79] Y. Montelongo, J. O. Tenorio-Pearl, C. Williams, S. Zhang, W. I. Milne, and T. D. Wilkinson, "Plasmonic nanoparticle scattering for color holograms," *Proceedings of the National Acadamy of Sciences of the United States of America*, vol. 111, no. 35, pp. 12679–12683, 2014.

[80] S. Larouche, Y.-J. Tsai, T. Tyler, N. M. Jokerst, and D. R. Smith, "Infrared metamaterial phase holograms," *Nature Materials*, vol. 11, no. 5, pp. 450–454, 2012.

[81] D. Wen, F. Yue, G. Li et al., "Helicity multiplexed broadband metasurface holograms," *Nature Communications*, vol. 6, no. 1, p. 8241, 2015.

[82] X. Zhang, J. Jin, Y. Wang et al., "Metasurface-based broadband hologram with high tolerance to fabrication errors," *Scientific Reports*, vol. 6, no. 1, p. 19856, 2016.

[83] H. Shi, C. Du, and X. Luo, "Focal length modulation based on a metallic slit surrounded with grooves in curved depths," *Applied Physics Letters*, vol. 91, no. 9, pp. 093111–093113, 2007.